J Mater Sci: Mater Electron (2015) 26:9907–9920
DOI 10.1007/s10854-015-3667-y

Dysprosium doped di-calcium magnesium di-silicate white light emitting phosphor by solid state reaction method

Ishwar Prasad Sahu[1] · D. P. Bisen[1] · Nameeta Brahme[1] · Raunak Kumar Tamrakar[2] · Ravi Shrivastava[3]

Received: 13 July 2015 / Accepted: 21 August 2015 / Published online: 30 August 2015

Abstract In this paper, we report the dysprosium doped di-calcium magnesium di-silicate namely $Ca_2MgSi_2O_7$:xDy^{3+} (x = 1.0, 1.5, 2.0, 2.5 and 3.0 mol%) phosphors were prepared by traditional high temperature solid state reaction method. Phosphors with optimum photo-luminescence intensity [$Ca_2MgSi_2O_7$:Dy^{3+} (2 %)] were characterized by X-ray diffraction (XRD) technique. The crystal structure of sintered phosphors were an akermanite type which belongs to the tetragonal crystallography with space group $P\overline{4}2_1m$. The chemical composition of the sintered phosphor $Ca_2MgSi_2O_7$:Dy^{3+} (2 %) was confirmed by the energy dispersive X-ray spectroscopy (EDS). Under the ultraviolet excitation, the emission spectra of $Ca_2MgSi_2O_7$:xDy^{3+} (x = 1.0, 1.5, 2.0, 2.5 and 3.0 mol%) phosphors were composed of broad band with the characteristic emission of Dy^{3+} ions are peaking at 475 nm (blue), 577 nm (yellow) and 678 nm (red), originating from the transitions of $^4F_{9/2} \rightarrow {}^6H_j$ state (where j = 15/2, 13/2, 11/2). The combination of these three emissions constituted white light as indicated on the Commission Internationale de l'Eclairage chromaticity diagram. The possible mechanism of the prepared white light emitting $Ca_2MgSi_2O_7$:xDy^{3+} (x = 1.0, 1.5, 2.0, 2.5 and 3.0 mol%) phosphors were also investigated. Investigation on decay property show that phosphor held fast and slow decay process. The peak of mechanoluminescence (ML) intensity increases linearly with increasing impact velocity of the moving piston, which suggests that this phosphor can be used as sensors to detect the stress of an object. Thus the present investigation indicates that piezo-electricity is responsible to produce ML in prepared phosphors.

1 Introduction

The alkaline earth (Sr, Ca, Ba) silicates containing rare earth ions are functional inorganic materials with strong luminescence in blue, green to red regions. These materials are widely used in the illumination, displays devices, storage devices, textile printing, exterior decoration, luminous paints and many more [1, 2]. To highlight a few one may include ''glow in dark items'' as; safe helmets, direction indicators and signs, plasma display panel, graphic arts, cathode ray tubes, vacuum fluorescent display, and the like due to their better physical and chemical stability, excellent photo resistance, very bright and long lasting afterglow with no radioactive radiations and hence forms the important materials in various ceramics industries [3, 4].

In recent years, alkaline earth silicates especially $Sr_2MgSi_2O_7$, $SrCaMgSi_2O_7$, $SrBaMgSi_2O_7$, $Ca_2MgSi_2O_7$, $Ba_2MgSi_2O_7$, $SrMgSi_2O_6$, $CaMgSi_2O_6$, Ba_2SiO_4, Sr_2SiO_4, Ca_2SiO_4, $SrSiO_3$ etc. doped with rare earth ions (Eu^{2+}, Dy^{3+} etc.) have been regarded as an excellent phosphor with high brightness and already in some commercial applications [5–7]. This has become possible due to their possessing broad and intense charge transfer (CT) bands or host absorption bands (HABs) in the near UV regions and thus they could efficiently transfer the absorbed energy to the activators (rare earth metal ions) by means of non-

✉ Ishwar Prasad Sahu
ishwarprasad1986@gmail.com

[1] School of Studies in Physics and Astrophysics, Pt. Ravishankar Shukla University, Raipur, C.G. 492010, India

[2] Department of Applied Physics, Bhilai Institute of Technology, Durg, C.G. 491001, India

[3] Department of Physics, ICFAI University, Raipur, C.G. 492001, India

radiative mechanisms [8, 9]. Thus, the silicate based phosphors has wide range of emissions depending on the doped rare earth ions and the host compositions. However, the emission color is mostly limited to the blue to red regions in these silicates. There are limited reports on efficient silicate phosphors that emits white light spectrum which is considered to be important for the various display devices [10].

Dysprosium (Dy^{3+}) is one of the important rare earth ions which play a major role in the production of different types of light emitting materials. The special interest in Dy^{3+} visible luminescence is due to the existence of two intense bands in the blue and yellow wavelength regions that, combined, will emit white light [11, 12]. The visible luminescence of Dy^{3+} ions mainly consists of two intense bands, one in the blue (460–480 nm) region and the other in the yellow (560–580 nm) region, which correspond to the $^4F_{9/2} \rightarrow {}^6H_{15/2}$ and $^4F_{9/2} \rightarrow {}^6H_{13/2}$ transitions. The interesting thing about the latter one is its hypersensitivity to the ligand environment of the Dy^{3+} ion. Also, at a suitable yellow to blue intensity ratio, the Dy^{3+} ions will emit white light [13]. Alkaline earth silicate based materials such as $Sr_2MgSi_2O_7$, $SrCaMgSi_2O_7$, $Ca_2MgSi_2O_7$ etc. also have strong mechanoluminescence (ML) and thermoluminescence (TL) properties. Currently, the ML phenomenon has attracted more attention because of its potential application for sensing structural damage, fractures, and deformation. Many efforts have been devoted to developing ML sensors due to their various applications such as visualization of stress, damage detection for air planes or cars, and the study of human diseases in the near future [14, 15].

In this paper, silicate was chosen as the host due to its special properties, such as low cost, easy preparation, excellent thermal and chemical stabilities, and especially the strong absorption in the near-UV region [16, 17]. Therefore, in this paper, we investigate the structural characterization and luminescent properties of dysprosium doped di-calcium magnesium di-silicate ($Ca_2MgSi_2O_7$:Dy^{3+}) phosphors with different concentration of Dy^{3+} ions (1.0, 1.5, 2.0, 2.5 and 3 mol%) by solid state reaction method. Solid state reaction method is widely used to prepare silicate based phosphors because samples prepared using this method has good luminescence intensity and very good morphology also. The crystal structure, chemical composition and different stretching modes were analyzed by X-ray diffractometer (XRD), energy dispersive X-ray spectroscopy (EDS) and fourier transform infrared (FTIR) spectra respectively. The luminescence properties were also investigated on the basis of thermoluminescence (TL), photoluminescence (PL), long afterglow (decay) and mechanoluminescence (ML) spectroscopy. Correlated color temperature (CCT) and color rendering index (CRI) was also calculated to check the suitability of practical white light source.

2 Experimental

2.1 Material preparation

The di-calcium magnesium di-silicate phosphors ($Ca_2MgSi_2O_7$) with different concentration (1, 1.5, 2, 2.5 and 3 mol%) of Dy^{3+} ions was prepared by the high temperature solid state reaction method. The raw materials are calcium carbonate [$CaCO_3$ (99.90 %)], magnesium oxide [MgO (99.90 %)], silicon di-oxide [SiO_2 (99.99 %)] and dysprosium oxide [Dy_2O_3 (99.99 %)], all of analytical grade (A.R.), were employed in this experiment. Small amount of boric acid (H_3BO_3) was added as flux. Initially, the raw materials were weighed according to the nominal compositions of $Ca_2MgSi_2O_7$:Dy^{3+} phosphors. Then the powders were mixed and milled thoroughly for 2 h using mortar and pestle. The chemical reaction used for stoichiometric calculation is:

$$4CaCO_3 + 2MgO + 4SiO_2 + 2Dy_2O_3 \xrightarrow{1200\,^{\circ}C} 2Ca_2MgSi_2O_7 : Dy^{3+} + 4CO_2 + 3O_2 \uparrow$$

The ground sample was placed in an alumina crucible and subsequently fired at 1200 °C for 3 h. At last the nominal compounds were obtained after the cooling down of programmable furnace and products were finally ground into powder for characterizing the phosphors.

2.2 Characterization techniques

The crystal structures of the prepared phosphors were characterized by powder XRD. Powder XRD pattern has been obtained from Bruker D8 advanced X-ray powder diffractometer and the data were collected over the 2θ range 10°–80°. The X-rays were produced using a sealed tube (CuKα) radiation source and the wavelength of X-ray was 1.54060 Å. The X-rays were detected using a fast counting detector based on Silicon strip technology (Bruker LynxEye detector). An EDS spectrum was used for the elemental (qualitative and quantitative) analysis of the prepared phosphors. FTIR spectra was recorded with the help of IR Prestige-21 by SHIMADZU for investigating the finger print region (1400–400 cm^{-1}), as well as the functional groups (4000–1400 cm^{-1}) of prepared phosphor in middle infrared region (4000–400 cm^{-1}) by mixing the sample with potassium bromide (KBr, IR grade). TL glow curves were recorded with the help of TLD reader 1009I by Nucleonix (Hyderabad, India Pvt. Ltd.). TL emission

spectrum was recorded with the help of different band pass interference (400–700 nm) filter. The excitation and emission spectra were recorded on a Shimadzu (RF 5301-PC) spectrofluorophotometer using the Xenon lamp (365 nm) as excitation source when measuring. The long afterglow (decay) curves were obtained using a Perkin Elmer fluorescent spectrometer with the proper excitation under a UV lamp (365 nm). The ML glow curve can be plotted with the help of SM-340 application software installed in a computer attached with the storage oscilloscope. All measurements were carried out at the room temperature.

3 Results and discussion

3.1 XRD analysis

In order to determine the crystal structure, powder XRD analysis has been carried out. The typical XRD patterns of $Ca_2MgSi_2O_7$ and $Ca_2MgSi_2O_7$:xDy^{3+} (x = 1.0, 1.5, 2.0, 2.5 and 3 mol%) phosphors with the standard XRD pattern were shown in Fig. 1a. Nearly, all the diffraction peaks of the resultant phosphors are consistent with Joint Committee Powder Diffraction Standard data (JCPDS) file (JCPDS: 77-1149) [18]. The position and intensity of diffraction peaks of resultant phosphors are well matched with the standard JCPDS file. It can be concluded that prepared phosphors are chemically and structurally $Ca_2MgSi_2O_7$ phosphors. From the XRD analysis of $Ca_2MgSi_2O_7$ and $Ca_2MgSi_2O_7$:xDy^{3+} (x = 1.0, 1.5, 2.0, 2.5 and 3 mol%) phosphors, it was found that the little amount of doped Dy^{3+} ions have no effect on the crystal structure of $Ca_2MgSi_2O_7$ phosphor.

Figure 1b shows the comparison between observed, calculated and standard (COD card No. 96-900-6452) XRD pattern of $Ca_2MgSi_2O_7$:Dy^{3+} (2 %) phosphor by MATCH 2 software. The Standard XRD pattern of $Ca_2MgSi_2O_7$ (COD card No. 96-900-6452) seems to show quite similar pattern as observed. The figure of merit (FOM) while matching these was 0.8989 (90 %) which illustrates that the crystal structure of the prepared sample agrees with the standard pattern COD card No. 96-900-6452. The $Ca_2MgSi_2O_7$ crystalline phase is nearly same a = b = 7.8470 Å, c = 5.0097 Å, α = 90°, β = 90°, γ = 90° and cell volume = 299.24 (Å)^3, Z = 2 is nearly same [a = b = 7.8350 Å and c = 5.0100 Å, α = 90°, β = 90°, γ = 90° and cell volume = 299.36 (Å)^3, Z = 2], with the standard lattice parameters which again signifies the proper preparation of the discussed $Ca_2MgSi_2O_7$:Dy^{3+} (2 %) phosphor. Hence, we conclude that the crystal structure of $Ca_2MgSi_2O_7$:xDy^{3+} (x = 1.0, 1.5, 2.0, 2.5 and 3 mol%) phosphors were an akermanite type structure which belongs to the tetragonal crystallography with space group $P\overline{42}_1m$ (113 space number and D^3_{2d} space group), this structure is member of the melilite group and forms a layered compound.

3.2 Energy dispersive X-ray spectroscopy (EDS)

Figure 2 shows an EDS spectrum of $Ca_2MgSi_2O_7$:Dy^{3+} (2 %) phosphor. The composition of the powder sample has been measured using an EDS spectrum. Table 1 shows the compositional (quantitative analysis) elements of $Ca_2MgSi_2O_7$:Dy^{3+} (2 %) phosphor, which is compare with the standard elements. An EDS is a standard procedure for identifying and quantifying elemental (chemical) composition of phosphors area, as small as a few nanometers. The elements appear in ratios concomitant with the proportions mixed in the starting materials, which is representing the composition of the powder sample.

The existence of dysprosium (Dy) in prepared $Ca_2MgSi_2O_7$:Dy^{3+} (2 %) phosphor was clear in an EDS spectrum. They revealed that there is no other emission apart from calcium (Ca), magnesium (Mg), silicon (Si) and oxygen (O) in the EDS spectra of the phosphor. In the EDS spectrum, intense peaks are present which confirm the presence of elements in $Ca_2MgSi_2O_7$:Dy^{3+} (2 %) phosphor.

3.3 Fourier transform infrared (FTIR) spectra

FTIR has been widely used for the identification of organic and inorganic compounds. The infrared spectrum of an inorganic compound represents its physical properties. Spectroscopically, the middle infrared region (4000–400 cm^{-1}) is extremely useful for the study of organic and inorganic compounds. Figure 3 shows the FTIR spectra of $Ca_2MgSi_2O_7$:Dy^{3+} (2 %) phosphor. In IR spectrum of $Ca_2MgSi_2O_7$:Dy^{3+} (2 %) phosphor, clearly exhibited broad bands in the region (3437.15 cm^{-1}) of hydroxyl group show the stretching vibration of hydroxyl (O–H) groups. The hydroxyl group in sintered phosphor is might be due to presence of moisture through environment. The asymmetric stretching of (CO_3^{2-}) carbonates can be observed in the range of 1900–1700 cm^{-1}. One weak shoulder, which corresponds to the out of plane bending, appears at approximately ~1919.32 cm^{-1}. These bands are due to a slight carbonation of the samples preparation [$CaCO_3$ (raw material)]. The vibration band around ~1635.04 cm^{-1} is assigned due to the Mg^{2+} [19].

In $Ca_2MgSi_2O_7$ crystal structure, the coordination number of calcium can be 6 and 8. Therefore, Ca^{2+} can occupy two alternative lattice sites, the eight coordinated Ca^{2+} site [CaO_8 (Ca_1 site)] and the six coordinated Ca^{2+} site [CaO_6 (Ca_2 site)] and other two independent cations sites, namely

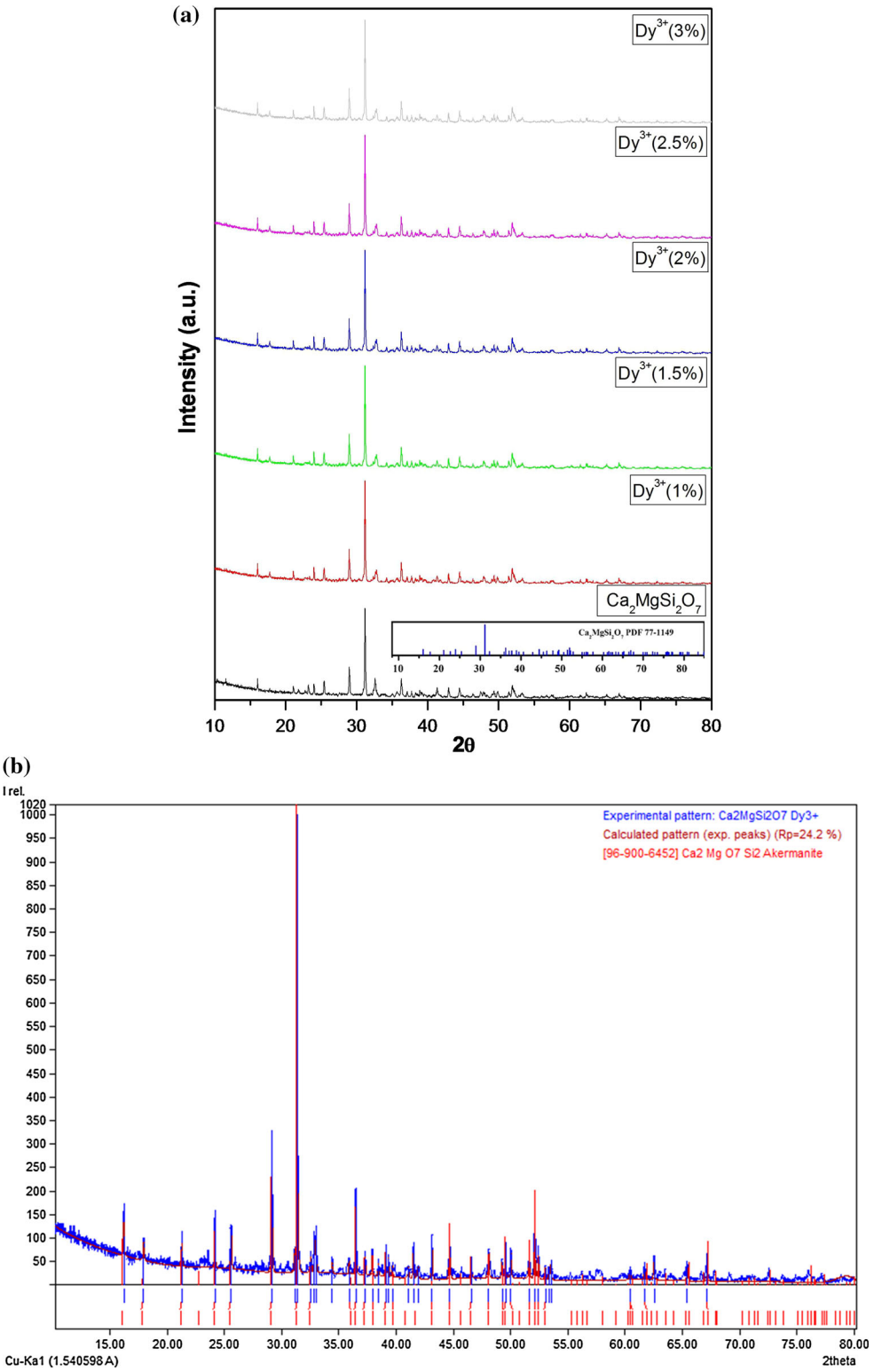

Fig. 1 **a** XRD pattern of $Ca_2MgSi_2O_7:Dy^{3+}$ phosphors with different Dy^{3+} concentration. **b** XRD pattern of $Ca_2MgSi_2O_7:Dy^{3+}$ (2 %) phosphor

Mg^{2+} [MgO_4], and Si^{4+} [SiO_4] also exist in the crystal lattice. Mg^{2+} and Si^{4+} cations occupy in the tetrahedral sites. When Dy^{3+} enters the lattice, it will only replace the original Ca^{2+} sites. So, Dy^{3+} will occupy four different lattice sites (Dy_1, Dy_2, Dy_3, and Dy_4) with coordination numbers of 6, 7, 8, and 9 [16, 17]. It's hard for Dy^{3+} ions to incorporate the tetrahedral [MgO_4] or [SiO_4] symmetry but it can easily incorporate octahedral [CaO_8] or hexahedral

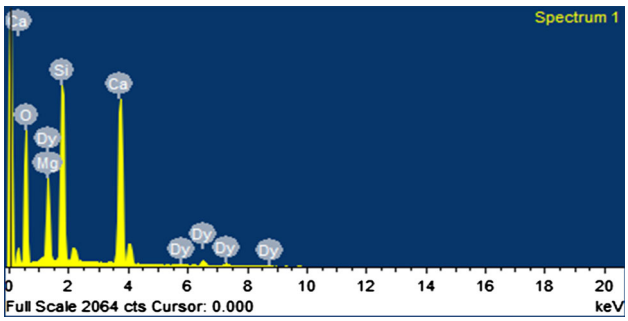

Fig. 2 EDS spectra of $Ca_2MgSi_2O_7:Dy^{3+}$ (2 %) phosphor

Table 1 Chemical composition of $Ca_2MgSi_2O_7:Dy^{3+}$ (2 %) phosphor

Sr. No.	Standard	Elements	Atomic (%)	Weight (%)
1	SiO_2	O K	43.18	64.17
2	MgO	Mg K	5.93	5.80
3	SiO_2	Si K	15.00	12.70
4	SrF_2	Ca L	27.02	16.03
5	DyF_3	Dy L	8.86	1.30
Total			99.99	99.99

$[CaO_6]$. Another fact that supports that the ionic radius of Dy^{3+} (0.99 Å) are very close to that of Ca^{2+} (about 1.12 Å) rather than Mg^{2+} (0.65 Å) and Si^{4+} (0.41 Å). Therefore, the Dy^{3+} ions are expected to occupy the Ca^{2+} sites in the $Ca_2MgSi_2O_7:Dy^{3+}$ (2 %) phosphor [20].

In the presented spectrum the absorption bands of silicate groups were clearly evident. The (Si–O_b–Si) and (Si–O_{nb}) stretching modes for the silicate tetrahedral show infrared absorption bands, located at about ~982.14, 941.26, 687.87 646.29 cm^{-1}. The two peaks in the finger print region ~846.20, 745.44 cm^{-1} are assigned due to the Ca^{2+} ions. The IR spectrum around ~493.76 cm^{-1} is based on the (Si–O–Si) bending modes as well as the Mg–O modes [21–23].

3.4 Thermoluminescence (TL)

TL is one of the possible ways to investigate the trap states of the materials. TL records glow intensity as a function of temperature, providing information regarding the trapping energies and the de-trapping mechanisms. TL in the phosphor is generated by the de-trapped carriers (holes and/or electrons) which recombine with the opposite carriers in the luminescent centers accompanied with the visible emission [24]. The traps created by the lattice defects play a very important role on the TL properties of the phosphors. The depth of trapping levels is very critical for the long afterglow phosphorescence. The photo induced electrons are released thermally and recombined with the holes. The initial irradiation by UV/VIS light is necessary to observe long phosphorescence [25, 26]. If the depth of trap is too shallow, the phosphor shows fast decay. On the contrary, if it is too deep, the phosphor does not show any phosphorescence at room temperature [27].

In order to study the trap states of the prepared $Ca_2MgSi_2O_7:xDy^{3+}$ (x = 1.0, 1.5, 2.0, 2.5 and 3 mol%) phosphors, TL glow curves were measured and are shown in Fig. 4a. The phosphors were first irradiated for 10 min

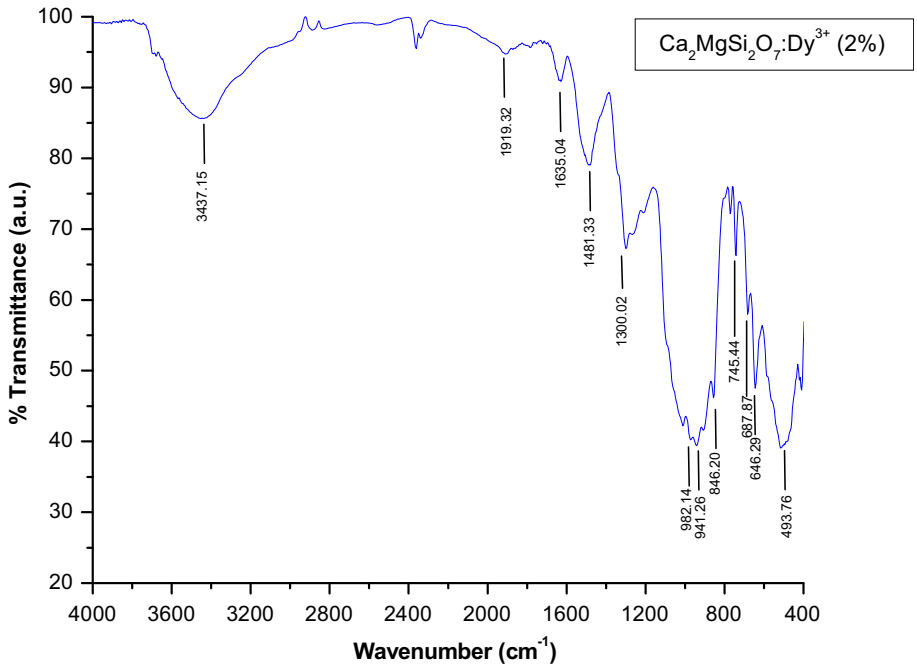

Fig. 3 FTIR spectra of $Ca_2MgSi_2O_7$: Dy^{3+} (2 %) phosphor

using 365 nm UV source, then the radiation source was removed and the irradiated samples were heated at a linear heating rate of 5 °C/s, from room temperatures to 300 °C. Initially the TL intensity increases with temperature, attains a peak value for a particular temperature, and then it decreases with further increase in temperature. A single glow peak of $Ca_2MgSi_2O_7$:xDy^{3+} (x = 1.0, 1.5, 2.0, 2.5 and 3 mol%) phosphors were obtained at 135.23 °C. The single isolated peak due to the formation of only one type of luminescence center which is created due to the UV irradiation. It is suggested that the recombination center associated with the glow at the temperature interval arises from the presence of liberated pairs, which are probably the results from the thermal release of electron/holes from different kinds of traps and recombine at the color centers [28, 29]. It is also known that the doping of the rare earth ions increases the lattice defects which have existed already in the host. It is readily observed that, intensity of TL signals increases with increase concentration of Dy^{3+} ions. It reaches optimum intensity when concentration of Dy^{3+} was 2.0 mol% then TL intensity decrease due to concentration quenching of Dy^{3+} ions. The different TL parameters are calculated and listed in Table 2.

Figure 4b shows the TL emission spectra of $Ca_2MgSi_2O_7$:Dy^{3+} (2 %) phosphor. TL emission spectra show a broad peak around 570 nm corresponds to yellow color in the visible region. TL emission spectrum confirms that the single isolated peak due to the formation of only one type of luminescence center.

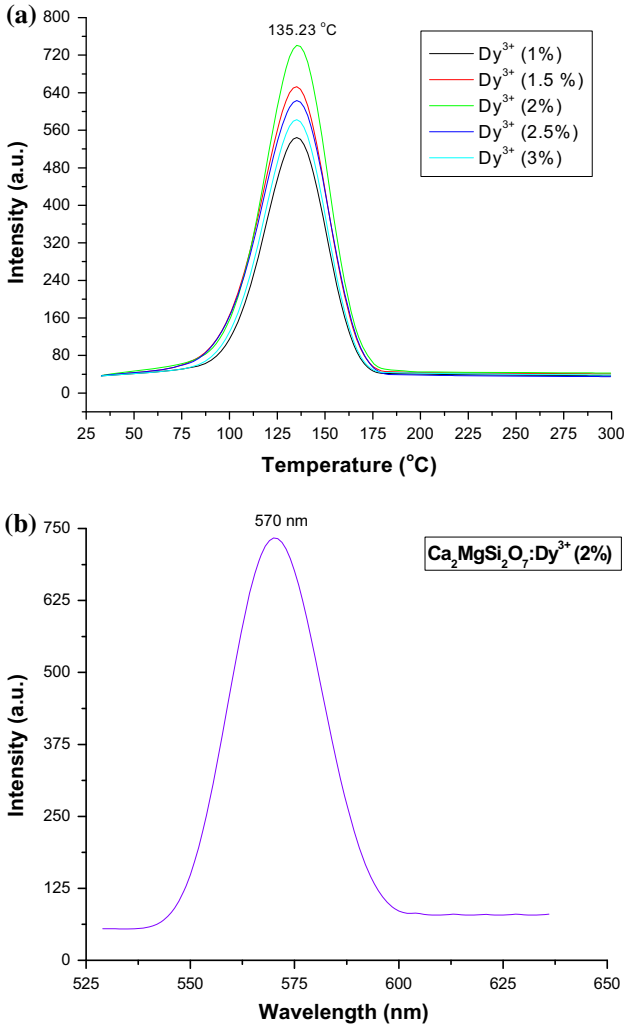

Fig. 4 **a** Comparative TL glow curve of $Ca_2MgSi_2O_7$:Dy^{3+} phosphors with different Dy^{3+} concentration. **b** TL emission spectra of $Ca_2MgSi_2O_7$:Dy^{3+} (2 %) phosphor

3.5 Determination of kinetic parameters

Measurement of the TL glow curves is one of the most useful ways to determine the number as well as the activation energy of the trapping levels in materials. The energy corresponding to the glow peak is equal to the trap depth. What has to be emphasized is that traps and carriers (electrons and holes) may be produced by irradiation, but they are also to be created during sample processing. Evaluation of kinetic parameters, i.e. the activation energy (E) of the traps involved in the TL emission, the order of kinetics (b), and the frequency factor (s), associated with the glow peaks of the thermally stimulated luminescence, is one of the most studied subjects in the field of condensed matter physics and a complete description of the thermoluminescent characteristics of a TL material requires to obtain these parameters. There are various methods for evaluating the trapping parameters from TL glow curves. For example, when one of the glow peaks is highly isolated from the others, the experimental method such as peak shape method is a suitable method to determine them from the glow peak. The TL parameters for the prominent glow peaks of prepared phosphor were calculated using the peak shape method are shown in Table 2 [30, 31]. The relationship between the frequency factor's' and the activation energy 'E' is given by the Eq. (1)

$$\frac{\beta E}{kT_m^2} = s\left[1 + (b-1)\frac{2kT_m}{E}\right]\exp(E/KT_{\mathrm{m}}) \quad (1)$$

where, k is Boltzmann constant, E is activation energy, b is order of kinetics, s is the frequency factor, T_m is temperature of peak position, and β is the heating rate. In the present work $\beta = 5\ \mathrm{Cs}^{-1}$. Trap depth for second order kinetics is calculated using the Eq. (2)

$$E = 2kT_m\left(1.76\frac{T_m}{\omega} - 1\right) \quad (2)$$

where, ω is the total half width intensity $\omega = \tau + \delta$, τ is the half width at the low temperature side of the peak ($\tau = \mathrm{T_m} - \mathrm{T_1}$); δ is the half width towards the fall-off side

Table 2 Activation energy (E), shape factor (μ_g) and frequency factor (s^{-1}) for 10 min UV irradiated $Ca_2MgSi_2O_7:Dy^{3+}$ phosphors for different Dy^{3+} concentration

Phosphors name	UV Min	HTR	T_1 (°C)	T_m (°C)	T_2 (°C)	τ (°C)	δ (°C)	ω (°C)	$\mu_g = \delta/\omega$	Activation energy	Frequency factor
$Ca_2MgSi_2O_7:Dy^{3+}$ (1.0 %)	10	5	114.07	135.23	154.57	21.16	19.34	40.50	0.48	1.17	1.89×10^{14}
$Ca_2MgSi_2O_7:Dy^{3+}$ (1.5 %)	10	5	112.12	135.23	154.47	23.11	19.24	42.35	0.45	1.12	3.84×10^{13}
$Ca_2MgSi_2O_7:Dy^{3+}$ (2.0 %)	10	5	114.07	135.23	155.27	21.16	20.04	41.20	0.49	1.15	1.02×10^{14}
$Ca_2MgSi_2O_7:Dy^{3+}$ (2.5 %)	10	5	112.57	135.23	154.36	22.66	19.13	41.79	0.46	1.13	6.14×10^{13}
$Ca_2MgSi_2O_7:Dy^{3+}$ (3.0 %)	10	5	113.06	135.23	154.47	22.17	19.24	41.41	0.46	1.15	8.50×10^{13}

of the glow peak ($\delta = T_2 - T_m$), T_m is the peak temperature at the maximum TL intensity T_1 and T_2 are, the temperatures on either side of T_m, corresponding to half intensity. The shape factor ($\mu_g = \delta/\omega$.) is to differentiate between first and second order TL glow peak. (μ_g) = 0.39–0.42 for the first order kinetics; (μ_g) = 0.49–0.52 for the second order kinetics and (μ_g) = 0.43–0.48 for the mixed order of kinetics [32, 33].

TL is an ideal technique in development and characterization of phosphors exhibiting persistence luminescence. Of course, in order to have strong afterglow, it is obvious that the trap density must be high [34]. Moreover another important factor for long lasting phosphors is producing a suitable trap depth within the host. If the trap depth is too low, the electrons in the trap can return to the energy level of the excited state easily, thus resulting in a short afterglow time. On the other hand if the trap depth is too deep the transition probability of electrons in the traps to the excited state is very low. In such a state the after glowing is less intense [35]. In our case, shape factor (μ_g) is lies between 0.45 to 0.49, which indicates that it is a case of non-first order kinetics, approaching towards second order, responsible for deeper trap depth.

3.6 Photoluminescence (PL)

In order to study the photo-luminescent properties, the excitation spectra of prepared $Ca_2MgSi_2O_7:Dy^{3+}$ (2 %) phosphor was recorded and shown in Fig. 5a. The excitation spectra were observed in the range of 200–400 nm and emission spectra was recorded in the range of 400–725 nm. The excitation spectrum in the range of 200–400 nm consists of the f → f transition of the Dy^{3+} ion. The excitation spectrum of $Ca_2MgSi_2O_7:Dy^{3+}$ (2 %) phosphor shows strong absorption at 352 nm and less intense absorptions at 248, 288 and 380 nm, which are ascribed to the transitions from the ground state to excitation states in the $4f^9$ configuration of Dy^{3+} but not easy to be clearly assigned due to the dense and somewhat overlapped levels of 4f configuration of Dy^{3+} in the high energy region. When the $Ca_2MgSi_2O_7:xDy^{3+}$ (x = 1.0, 1.5, 2.0, 2.5 and 3 mol%) phosphors were excited at 352 nm, simultaneous emissions of blue (475 nm), yellow (577 nm) and red (678) nm position were observed. Notice that the red emission is less intense than the blue and yellow emissions. These three different emission bands originated from the one origin owing to their having the same excitation wavelength. The transitions involved in blue, yellow and red bands of Dy^{3+} ion are well known and have been identified as $^4F_{9/2} \rightarrow {}^6H_{15/2}$, $^4F_{9/2} \rightarrow {}^6H_{13/2}$ and $^4F_{9/2} \rightarrow {}^6H_{11/2}$ transitions respectively. One can also find that the emission lines of Dy^{3+} are broadened somewhat because there are several Stark levels for the $^4F_{9/2} \rightarrow {}^6H_J$ levels [36].

Figure 5b shows that the emission spectra of $Ca_2MgSi_2O_7:Dy^{3+}$ phosphors with different Dy^{3+} concentration. It is well known that the former weak blue emission at 475 nm ($^4F_{9/2} \rightarrow {}^6H_{15/2}$) is corresponded to the magnetic dipole transition, which hardly varies with the crystal field strength around Dy^{3+}. While the later stronger yellow emission at 577 nm ($^4F_{9/2} \rightarrow {}^6H_{13/2}$) belongs to the hypersensitive forced electric dipole transition, which is strongly influenced by the outside surrounding environment [37]. According to the Judd–Ofelt theory [29], when Dy^{3+} locates at a low symmetry local site (without inversion symmetry), a yellow emission according to the electric dipole transition ($^4F_{9/2} \rightarrow {}^6H_{13/2}$) will be dominant. Conversely, a magnetic dipole transition ($^4F_{9/2} \rightarrow {}^6H_{15/2}$) will predominate in the emission spectra, resulting in a strong blue emission. In our case, the yellow emission ($^4F_{9/2} \rightarrow {}^6H_{13/2}$) will dominate. The strong yellow emission is also beneficial to decrease the color temperature of the

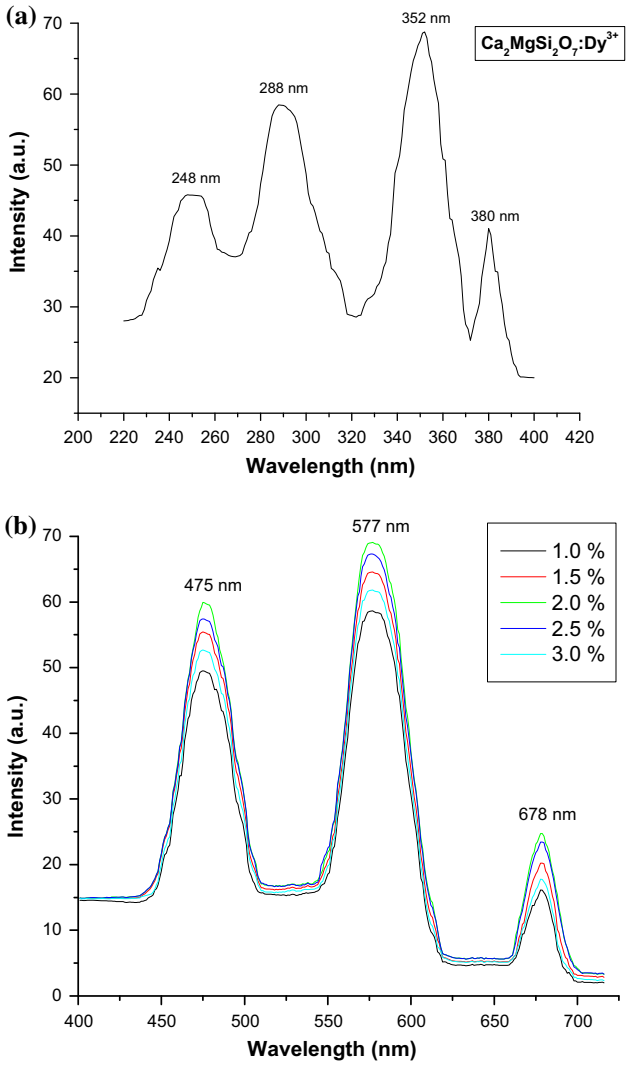

Fig. 5 **a** Excitation spectra of $Ca_2MgSi_2O_7:Dy^{3+}$ phosphor. **b** Emission spectra of $Ca_2MgSi_2O_7:Dy^{3+}$ phosphors with different Dy^{3+} concentration

phosphor and generate warm white light emission. Moreover, the hardly perceptible transition ($^4F_{9/2} \rightarrow {}^6H_{11/2}$) emission at 678 nm can be observed, which is also due to the disordered crystal field and is corresponding to the structural study. It is notice that the red emission is less intense than the blue and yellow emissions. It is well known that the ($^4F_{9/2} \rightarrow {}^6H_{13/2}$) transition is hypersensitive and therefore, its intensity strongly depends on the host, while the ($^4F_{9/2} \rightarrow {}^6H_{15/2}$) transition is less sensitive to the host. The optical properties of the material are often influenced by the structure of the matrix and synthesis technique [38].

When trivalent metallic ions, such as Dy^{3+} are incorporated into a host lattice and substitute divalent metallic ions, the charge balancing is necessarily required. Due to these chemically nonequivalent substitutions, an excess of positive charge in the host lattice must be compensated. One possible way of charge compensation mechanism is that two Dy^{3+} ions replace three Ca^{2+} ions to balance the charge of these phosphors, which create two $Dy_{Ca}^{\cdot}$ positive defects and one V_{Ca}'' negative defect.

$$2Dy^{3+} + 3Ca^{2+} \rightarrow 2Dy_{Ca}^{\cdot} + V_{Ca}'' \quad (3)$$

For $Ca_2MgSi_2O_7:Dy^{3+}$ the incorporation of alkali metal ions can neutralize the charge generated by Dy^{3+} substitution for Ca^{2+}, and thus stabilize the structure and enhance the luminescence. Dy^{3+} ions have been often used as co-dopants in the previously developed aluminate and silicate based materials. When divalent alkaline earth ions, such as Ca^{2+} or Sr^{2+} or Ba^{2+} is substituted by trivalent Dy^{3+} in the alkaline earth silicates and aluminates, various defects can be induced due to the charge compensation mechanism. However, in Dy^{3+} singly doped samples, which are in our current interest, Dy^{3+} is not only the supplier of traps but also an activator itself [16, 17].

A process of emitting the white light in $Ca_2MgSi_2O_7:Dy^{3+}$ phosphor is illustrated schematically in Fig. 6. After irradiation with the ultraviolet light ([1]), most of the excitation energy associated with the excited carriers (electrons or holes) will be transferred via the host directly to the luminescence centers, Dy^{3+}, followed by the Dy^{3+} 4f emissions as the immediate luminescence ([39]). However, part of the excitation energy will be stored when some of the excited carriers drop into the traps ([2]), instead of returning to the ground states. Later, with thermal excitation at proper temperature, these carriers will be released from the traps and transferred via the host to the Dy^{3+} ions, followed by the characteristic Dy^{3+} emissions as long afterglow ([3]). In the practical system, the electron traps and the hole traps may not be both equally abundant

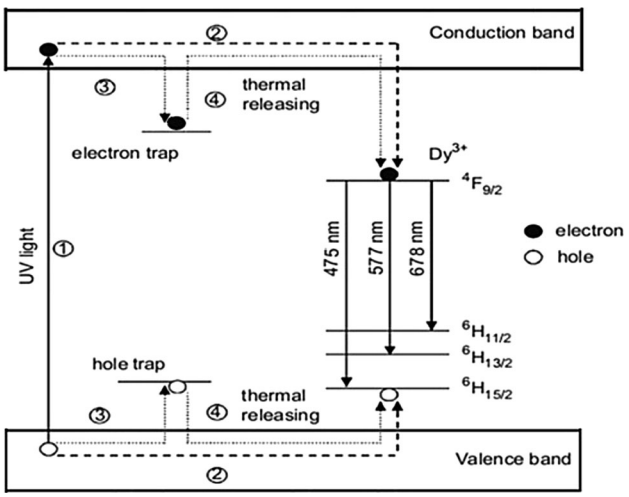

Fig. 6 Schematic diagram of the mechanism in $Ca_2MgSi_2O_7:Dy^{3+}$ phosphor

or important in terms of their contribution to the white light emission, as suggested in Fig. 6 [16, 17, 40].

To investigate the concentration dependent luminescent property of Dy^{3+} ions doped $Ca_2MgSi_2O_7$ host, a series of $Ca_2MgSi_2O_7$:xDy^{3+} (x = 1.0, 1.5, 2.0, 2.5 and 3.0 %) phosphors were synthesized and the luminescent properties were measured are shown in Fig. 5b. It can be seen that all the emission spectra are similar regardless of Dy^{3+} contents. As the concentration x increases, the intensity of Dy^{3+} emission increases and reaches a maximum at 2 % and then decreases when Dy^{3+} content further increases due to the concentration quenching effect. Concentration quenching is mainly caused by energy transfer among Dy^{3+} ions in the host lattice, the probability of which increases as the concentration of Dy^{3+} increases [41].

3.7 CIE chromaticity coordinate

In general, color of any phosphor material is represented by means of color coordinates. The luminescence color of the samples excited under 352 nm has been characterized by the CIE (Commission International de I'Eclairage) 1931 chromaticity diagram. [42] The emission spectrum of the $Ca_2MgSi_2O_7$:Dy^{3+} (2 %) phosphor was converted to the CIE 1931 chromaticity using the photo-luminescent data and the interactive CIE software (CIE coordinate calculator) diagram as shown in Fig. 7.

Every natural color can be identified by (x, y) coordinates that are disposed inside the 'chromatic shoe' representing the saturated colors. [43] Luminescence colors of

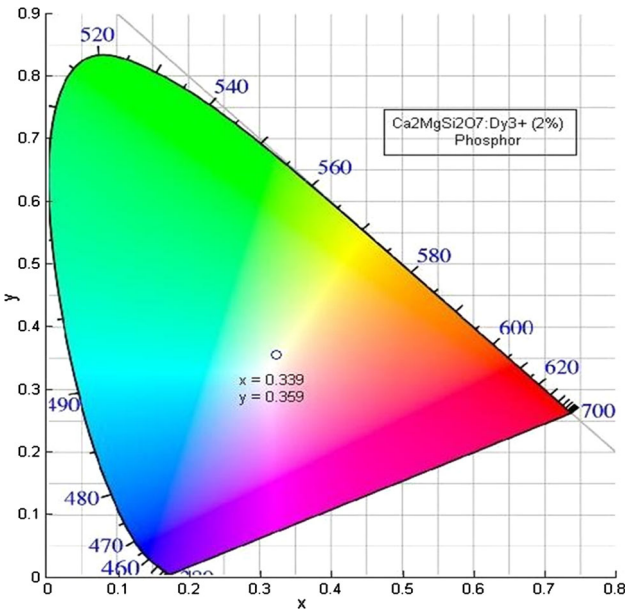

Fig. 7 CIE chromaticity diagram of $Ca_2MgSi_2O_7$:Dy^{3+} (2 %) phosphor

$Ca_2MgSi_2O_7$:Dy^{3+} (2 %) phosphor are placed in the (x = 0.339, y = 0.359), which is represented by the circle symbol ["o"]. The chromatic co-ordinates of the luminescence of this phosphor are measure and reached near to white luminescence. The interaction between Dy^{3+} ion and host lattice follows the proposed CEI model and emission colors are located between the three extreme points corresponding to the CEI model i.e. near to white light emission could be investigated, which is in the good agreement with the chromaticity coordinates of standard white light (x = 0.333, y = 0.333) [16, 17]. The calculated CIE values of other concentration of $Ca_2MgSi_2O_7$:xDy^{3+} (x = 1.0, 1.5, 2.5 and 3 mol%) phosphors were listed in Table 3.

3.8 Correlated color temperature (CCT)

CCT relates to the color of light produced by a light source, measured in degrees Kelvin. The CCT rating is an indication of how "warm" or "cool" the light source appears. The higher the CCT value, the cooler the lamp color will appear. The lower the number, the warmer the lamp color will appear. However, CCT is only one aspect of color. However, opposite to the temperature scale, lamps with a CCT rating below 3200 K are usually considered ''warm'' sources, while those with a CCT above 4000 K are usually considered ''cool'' in appearance. McCamy has proposed the analytical equation to calculate the CCT which is given [44] by

$$CCT = -449n^3 + 3525n^2 - 6823n + 5520.33 \quad (4)$$

where, $n = (x-x_e)/(y-y_e)$ is the inverse slope line and ($x_e = 0.332$, $y_e = 0.186$) is the epicenter. Generally, the preferred CCT values range from 4000 to 6500 K but the range from 3500 to 7500 K may also be accepted. The calculated CCT values of prepare $Ca_2MgSi_2O_7$:Dy^{3+} (2 %) phosphor is 5250 K, which is well under the acceptable ranged and can be considered ''cool'' in appearance. The calculated CCT values of other concentration of $Ca_2MgSi_2O_7$:xDy^{3+} (x = 1.0, 1.5, 2.5 and 3 mol%) is listed in Table 3. It can be seen that the value of CCT varies from 5288 to 5442 K, which is well under the acceptable ranged and can be considered ''cool'' in appearance [45].

3.9 Color rendering index (CRI)

The CRI, sometimes called color rendition index, is a quantitative measurement of the ability of a light source to reveal the colors of various objects faithfully in comparison with an ideal or natural light source. The ability of any given light source to represent colors in objects is its CRI. It is based on a relative measurement which will rate light sources on a scale of 0–100 [41, 42]. The higher the CRI,

Table 3 CCT and CRI calculation of $Ca_2MgSi_2O_7:Dy^{3+}$ phosphors for different Dy^{3+} concentration

Sr No.	Phosphors name	Peak intensity	CIE chromaticity Co-ordinates		CCT (K)	CRI
			x	y		
1	$Ca_2MgSi_2O_7:Dy^{3+}$ (1.0 %)	58.638	0.334	0.359	5442	65.4896
2	$Ca_2MgSi_2O_7:Dy^{3+}$ (1.5 %)	64.568	0.335	0.357	5402	65.8531
3	$Ca_2MgSi_2O_7:Dy^{3+}$ (2.0 %)	69.068	0.339	0.359	5250	66.0777
4	$Ca_2MgSi_2O_7:Dy^{3+}$ (2.5 %)	67.318	0.338	0.359	5288	66.5486
5	$Ca_2MgSi_2O_7:Dy^{3+}$ (3.0 %)	61.818	0.335	0.358	5402	65.7955

the more natural the colors appear. A higher CRI means better color rendering, or less color shift. CRIs in the range of 75–100 are considered excellent, while 65–75 are good. The range of 55–65 is fair, and 0–55 is poor [46]. The values of CRI were also calculated in our experiment. The calculated CRI of prepare $Ca_2MgSi_2O_7:Dy^{3+}$ (2 %) phosphor is 66.07, which is again in the preferable range. The values of CRI were also calculated and listed in Table 3. CRI of different samples varies from 65.48 to 65.85, which is again well under the preferable range.

3.10 Long afterglow (decay)

Figure 8 shows the typical decay curves of $Ca_2MgSi_2O_7:Dy^{3+}$ (2 %) phosphor. The initial afterglow intensity of the sample was high. The decay times of phosphor can be calculated by a curve fitting technique, and the decay curves fitted by the sum of two exponential components have different decay times [47].

$$I = A_1 \exp(-t/\tau_1) + A_2 \exp(-t/\tau_2) \quad (5)$$

where, I is phosphorescence intensity, A_1, A_2 are constants, t is time, τ_1 and τ_2 are decay times (in second) for the exponential components. Decay curves are successfully fitted by the Eq. (5) and the fitting curve result are shown in Table 4. The results indicated that the, afterglow decay curves are composed of two regimes, i.e., the initial rapid decaying process and the subsequent slow decaying process.

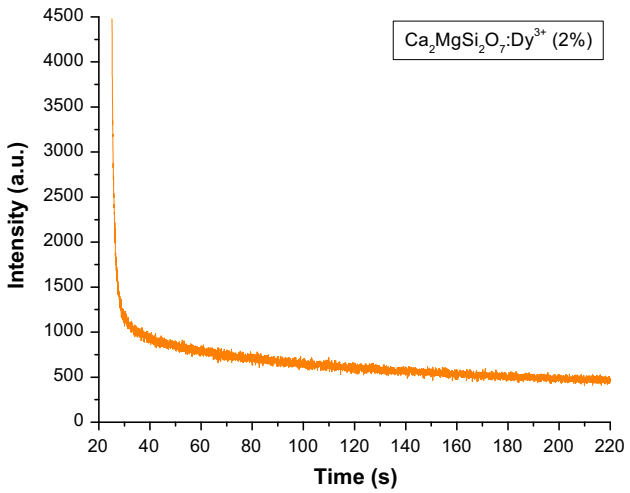

Fig. 8 Decay curve of $Ca_2MgSi_2O_7:Dy^{3+}$ (2 %) phosphor

Dy^{3+} is an important rare earth ion in the development of phosphors with long lasting afterglow, playing a crucial role. The dopant Dy^{3+} is a famous trap creating ion, which can greatly prolong the afterglow. It is reasonable to consider that the role of doping Dy^{3+} ions is to introduce new types of traps or significantly increase the concentration of traps responsible for the afterglow [48]. The afterglow intensity of the persistent phosphor depends on the densities of the traps electrons, while the duration of afterglow depends on the depth of the trapped electrons. The number of trapped charge carrier, in term, depends on the concentration of oxygen vacancies/Dy^{3+} and the trap depth of it. For a suitable trap depth, the trap concentration is directly depends on the dysprosium ions [49] (Table 5).

3.11 Mechanoluminecsnce (ML)

Mechanoluminescence (ML) (also known as Triboluminescence) is an important physical phenomenon where an emission of light is observed due to mechanical deformation of materials, when they are subjected to some mechanical stress like rubbing, cleavage, compressing, impulsive deformation, crushing, grinding, shaking etc. This phenomenon has been observed in many kinds of solids including ionic crystals, semiconductors, metals, glasses and organic crystals [50, 51]. In the present ML studies, an impulsive deformation technique has been used. When a moving piston (load) is applied on to the phosphor, initially the ML intensity increases with time, attains a

Table 4 Fitting results of the decay curves

Phosphor	τ_1 (s)	τ_2 (s)
$Ca_2MgSi_2O_7:Dy^{3+}$ (2 %)	1.18	62.16

Table 5 Calculation of ML decay constant for $Ca_2MgSi_2O_7:Dy^{3+}$ (2 %) phosphor

Impact velocity	10 cm	20 cm	30 cm	40 cm	50 cm
τ Decay constant (ms)	0.80	0.81	0.82	0.85	0.90

peak value and then it decreases with time. Such a curve between the ML intensity and deformation time of a solid is known as the ML glow curve. During the deformation of a solid, a great number of physical processes may occur within very short time intervals, which may excite or stimulate the process of photon emission [52].

Figure 9 shows that the characteristics curve between ML intensity versus time for different heights (h = 10, 20, 30, 40, 50 cm). The phosphor was fracture via dropping a load [moving piston] of particular mass (400 g) and cylindrical shape on the $Ca_2MgSi_2O_7:Dy^{3+}$ (2 %) phosphor. The velocity of the moving piston, holding the impact mass, could be changed, by changing the height through which it was dropped. Every time for the ML measurement, the quantity of $Ca_2MgSi_2O_7:Dy^{3+}$ (2 %) phosphor was kept constant (8 mg). When prepared $Ca_2MgSi_2O_7:Dy^{3+}$ (2 %) phosphor was fractured, free electrons and holes are generated, which may excite or stimulate the process of light emission. In these ML experiment, the maximum ML intensity has been obtained for the 50 cm dropping height of moving piston. The prepared $Ca_2MgSi_2O_7:Dy^{3+}$ (2 %) phosphor was not irradiated by any excitation source such as Ultra-Violet, Laser, X-ray, β-rays or γ-rays. From Fig. 9 it can be seen that the linearly increase of compressive height can induce the increase of ML intensity. That is, the ML intensity of $Ca_2MgSi_2O_7:Dy^{3+}$ (2 %) phosphor was linearly proportional to the magnitude of the impact velocity of moving piston.

Figure 9 (inset) shows the curve of the ML intensity of $Ca_2MgSi_2O_7:Dy^{3+}$ (2 %) phosphor for different impact velocities. It is seen that, ML intensity increases linearly with increasing impact velocity [$\upsilon_0 = \sqrt{2gh}$ (where, $\boldsymbol{g}$ is the acceleration due to gravity and $\boldsymbol{h}$ is the height through which the load was dropped)] of the moving piston. The ML intensity of $Ca_2MgSi_2O_7:Dy^{3+}$ (2 %) phosphor increases with increasing the mechanical stress [53]. Figure 10 comparative ML intensity versus time of $Ca_2MgSi_2O_7:Dy^{3+}$ phosphors with different Dy^{3+} concentration for 50 cm height. It is seen that ML intensity increase with increasing concentration of Dy^{3+} ions. It reaches optimum intensity when concentration of Dy^{3+} was 2.0 mol%, then ML intensity decrease due to concentration quenching of Dy^{3+} ions.

When the load or piston makes an impact on the crystal with an initial velocity v_0, the former decelerates and after a particular time its velocity becomes zero. The time dependence of the velocity of the piston may be written as

$$v = v_0 \exp(-\beta v_o t) \tag{6}$$

where β is a constant, Eq. (6) can be written as

$$\frac{dx}{dt} = v_0 \exp(-\beta v_o t) \tag{7}$$

where dx is the compression of the crystal during the time interval dt.

Integrating Eq. (7), we have

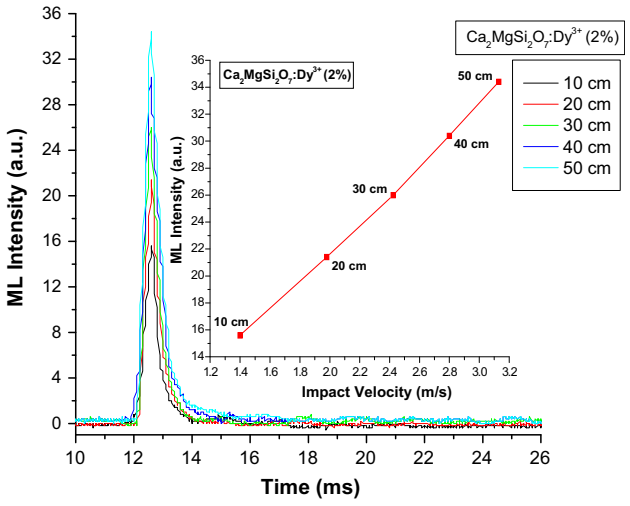

Fig. 9 ML intensity versus time of $Ca_2MgSi_2O_7:Dy^{3+}$ (2 %) phosphor (*Inset*—ML intensity vs. impact velocity of $Ca_2MgSi_2O_7:Dy^{3+}$ (2 %) phosphor)

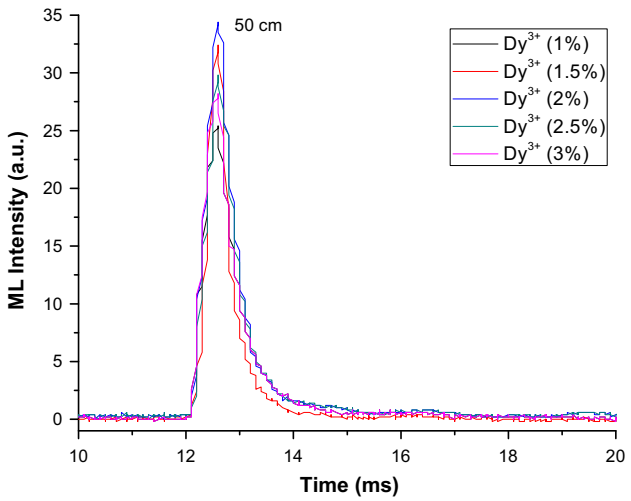

Fig. 10 Comparative ML intensity versus time of $Ca_2MgSi_2O_7:Dy^{3+}$ phosphors with different Dy^{3+} concentration for 50 cm height

$$x = \frac{1}{\beta}\exp(-\beta v_o t) + C \tag{8}$$

x = 0 for t = 0, therefore, Eq. (8) may be written as

$$x = \frac{1}{\beta}[1 - \exp(-\beta v_o t)] \tag{9}$$

The phosphor is in powder form and the impact velocities compress it to a certain extent, but this does not change significantly with increasing impact velocity. Equation (9) shows that impact time remains mostly unchanged with increasing impact velocity because there is no significant change in compression, which is expressed by 'x' in Eq. (8). This may be one possible reason why the time that corresponds to the peak ML intensity does not change significantly with increasing impact velocity [54]. Figure 11 shows the time corresponds to ML signal peak with impact velocity of $Ca_2MgSi_2O_7:Dy^{3+}$ (2 %) phosphor.

The relationship between semi-log plot of ML intensity versus $(t-t_m)$ for $Ca_2MgSi_2O_7:Dy^{3+}$ (2 %) phosphor was shown in Fig. 12, and the lines were fitted using the following Eq. (10) with Origin Pro 8.0

$$\tau = \frac{1}{slop\ of\ straight\ line} \tag{10}$$

Curve fitting results show that decay constant (τ) varies from 0.80 to 0.90 ms. The ML decay constant value was increases with the impact velocities, and maximum for the maximum impact velocities.

When a mechanical stress, such as compress, friction, and striking, and so on, was applied on the sintered phosphors, piezo-electric field can be produced. Previous researches have revealed that the prepared $Ca_2MgSi_2O_7:Dy^{3+}$ (2 %) phosphor has a tetragonal structure with space group $P\overline{42}_1m$, possesses piezo-electrification. Therefore, in such crystallites the ML excitation may be caused by the local piezoelectric field near the impurities and defects in the crystals. During the impact of the sample, one of its newly created surfaces gets positively charged and the other surface of the crack gets negatively charged [Fig. 13 Langevin model]. Thus, an intense electric field of the order of 10^6–10^7 Volt cm^{-1} is produced. [55] Under such order of electric field, the ejected electrons from the negatively charged surface may be accelerated and subsequently their impact on the positively charged surfaces may excite the luminescence center. Thus, depending on the prevailing conditions, recombination luminescence may be produced. For the impact velocity υ_0, the impact pressure P_0 will be equals to, $P_0 = Z\upsilon_0$, where Z is a constant. As the impact velocity increases, the impact pressure also increases leading to the increase in the electric field at local region which causes the decrease in trap depth. Hence the probability of de-trapping increases. Thus, the ML intensity will increase linearly with increasing value of impact velocity (υ_0).

As the impact velocity increases, the impact pressure also increases leading to the increase in the electric field at local region which causes the decrease in trap depth. Hence the probability of de-trapping increases. From Fig. 9 (inset), it can be seen that with increasing impact velocity, ML intensity also increases linearly i.e., the ML intensity of $Ca_2MgSi_2O_7:Dy^{3+}$ (2 %) phosphor was lineally proportional to the magnitude of the impact velocity. When the surface of an object was coated with the ML materials, the stress distribution in the object beneath the layer could be reflected by the ML brightness and could be observed.

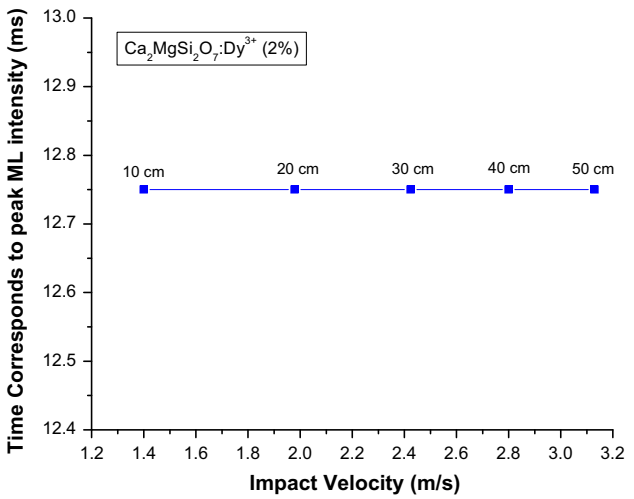

Fig. 11 Time corresponds to ML signal peak with impact velocity of $Ca_2MgSi_2O_7:Dy^{3+}$ (2 %) phosphor

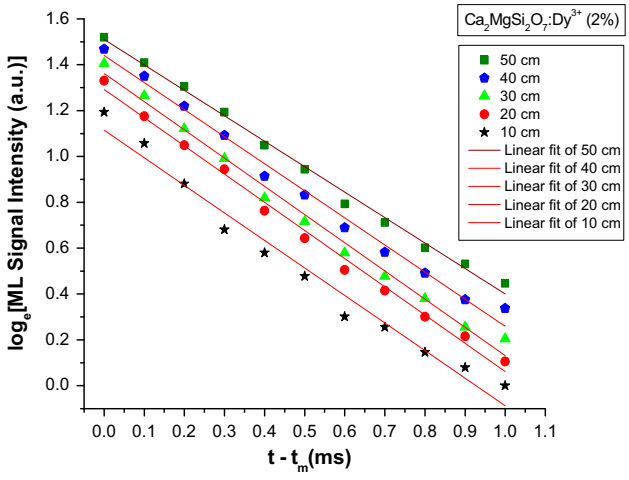

Fig. 12 Semi-log plot of ML intensity versus $(t-t_m)$ for $Ca_2MgSi_2O_7:Dy^{3+}$ (2 %) phosphor

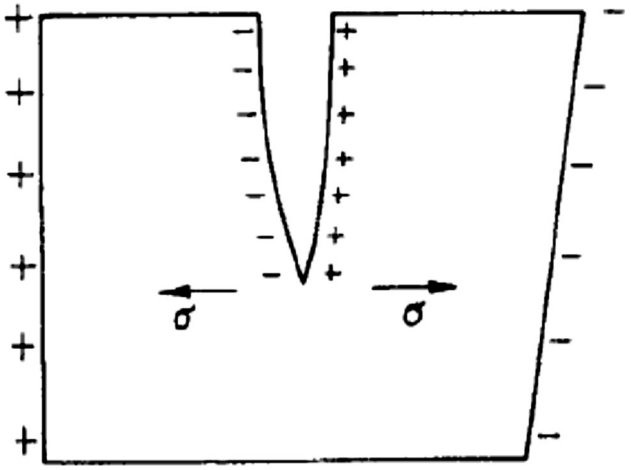

Fig. 13 Langevin model for the piezo-electrification induce phosphor

Based on the above analysis these phosphors can also be used as sensors to detect the stress of an object [56–60].

4 Conclusion

In summary, a new potential dysprosium doped white light emitting di-calcium magnesium di-silicate ($Ca_2MgSi_2O_7$:Dy^{3+}) phosphors with different concentration of Dy^{3+} (1.0, 1.5, 2.0, 2.5 and 3 mol%) were successfully synthesized by the solid state reaction method. The crystal structure of the sintered $Ca_2MgSi_2O_7$:xDy^{3+} (x = 1.0, 1.5, 2.0, 2.5 and 3 mol%) phosphors were consistent with standard tetragonal crystallography. The EDS spectra confirm the chemical composition of $Ca_2MgSi_2O_7$:Dy^{3+} (2 %) phosphor. TL, PL and ML intensity increases with increasing concentration of Dy^{3+} ions. It reaches optimum intensity when concentration of Dy^{3+} ions was 2.0 mol%, then TL, PL and ML intensity decrease due to concentration quenching of Dy^{3+} ions. Under the ultra-violet excitation, the prepared $Ca_2MgSi_2O_7$:xDy^{3+} (x = 1.0, 1.5, 2.0, 2.5 and 3 mol%) phosphors would emit blue, yellow and red light with peak at 475 nm, 577 nm and 678 nm corresponds to the transitions of $^4F_{9/2} \rightarrow {}^6H_{15/2}$, $^4F_{9/2} \rightarrow {}^6H_{13/2}$ and $^4F_{9/2} \rightarrow {}^6H_{11/2}$ respectively. PL emission of all the phosphors exhibited white light for human eyes which was confirmed from the calculated CIE coordinates. The ML intensity of $Ca_2MgSi_2O_7$:Dy^{3+} (2 %) phosphor strongly depends on the impact velocity of the moving piston which is used to deform the sample and a linear relationship between the ML intensity and impact velocity exists. Based on the above analysis this phosphor can also be used as sensors to detect the stress of an object.

Acknowledgments "We are very grateful to UGC-DAE Consortium for Scientific Research, Indore (M.P.) for the XRD Characterization and we are very thankful Dr. Mukul Gupta for his co-operation". We are very thankful to Dr. K.V.R. Murthy, Department of Applied physics, M.S. University Baroda, Vadodara (Gujarat) India for the photoluminescence study.

References

1. H. Wu, Y. Hu, Y. Wang, C. Fu, J. Alloys Compd. **497**, 330–335 (2010)
2. Y. Chen, B. Liu, M. Kirm, Z. Qi, C. Shi, M. True, S. Vielhauer, G. Zimmerer, J. Lumin. **118**, 70–78 (2006)
3. Y. Xu, D. Chen, Ceram. Int. **34**, 2117–2120 (2008)
4. W. Pan, G. Ning, X. Zhang, J. Wang, Y. Lin, J. Ye, J. Lumin. **128**, 1975–1979 (2008)
5. I.P. Sahu, D.P. Bisen, N. Brahme, R.K. Tamrakar, R. Shrivastava, Res. Chem. Intermed. (2015). doi:10.1007/s11164-015-2120-4
6. Y. Gong, Y. Wang, Z. Jiang, X. Xu, Y. Li, Mater. Res. Bull. **44**, 1916–1919 (2009)
7. I.P. Sahu, J. Mater. Sci.: Mater. Electron. (2015). doi:10.1007/s10854-015-3327-2
8. B. Liu, C. Shi, M. Yin, L. Dong, Z. Xiao, J. Alloys Compd. **387**, 65–69 (2005)
9. C. Fu, Y. Hu, Y. Wang, H. Wu, X. Wang, J. Alloys Compd. **502**, 423–428 (2010)
10. V.C. Teixeira, P.J.R. Montes, M.E.G. Valerio, Opt. Mater. **36**, 1580–1590 (2014)
11. Y. Ding, Y. Zhang, Z. Wang, W. Li, D. Mao, H. Han, C. Chang, J. Lumin. **129**, 294–299 (2009)
12. M.A. Tshabalalaa, F.B. Dejene, S.S. Pitale, H.C. Swart, O.M. Ntwaeaborwa, Phys. B **439**, 126–129 (2014)
13. S.K. Gupta, M. Kumar, V. Natarajan, S.V. Godbole, Opt. Mater. **35**, 2320–2328 (2013)
14. C.N. Xu, H. Yamada, X. Wang, X.G. Zheng, Appl. Phys. Lett. **84**, 3040–3042 (2004)
15. C.N. Xu, X.G. Zheng, T. Wantanabe, M. Akiyama, I. Usui, Thin Solid Films **352**, 273–278 (1999)
16. I.P. Sahu, D.P. Bisen, N. Brahme, Displays **38**, 68–76 (2015)
17. I.P. Sahu, D.P. Bisen, N. Brahme, Displays **35**, 279–286 (2014)
18. JCPDS file number 77-1149, JCPDS International Center for Diffraction Data
19. M.A. Salim, R. Hussain, M.S. Abdullah, S. Abdullah, N.S. Alias, S.A. Ahmad Fuzi, M.N. Md Yusuf, K.M. Mahbor, Solid State Sci. Technol. **17**, 59–64 (2009)
20. I.P. Sahu, D.P. Bisen, N. Brahme, L. Wanjari, R.K. Tamrakar, Res. Chem. Intermed. (2015). doi:10.1007/s11164-015-1929-1
21. C. Chang, D. Mao, J. Alloys Compd. **390**, 134 (2005)
22. G. T. Chandrappa, S. Ghosh, K. C. Patil, J. Mater. Syn. Process. 72–73 (1999)
23. I.P. Sahu, D.P. Bisen, N. Brahme, Lumin. J. Biol. Chem. Lumin. (2015). doi:10.1002/bio.2869
24. J. Qiu, K. Miura, H. Inouye, Appl. Phys. Lett. **73**, 1763–1765 (1998)
25. C.Y. Li, Y.N. Yu, S.B. Wang, Q. Su, J. Non-Cryst. Solids **321**, 191–196 (2003)
26. A. Nag, T.R.N. Kutty, Mater. Res. Bull. **39**, 331–342 (2004)
27. T. Katsumata, R. Sakai, S. Komuro, T. Morikawa, J. Electrochem. Soc. **150**, 111–114 (2003)
28. H.N. Luitel, T. Watari, R. Chand, T. Torikai, M. Yada, J. Mater. **2013**, 10 (2013)
29. J. Wang, S. Wang, Q. Su, J. Solid State Chem. **177**, 895 (2004)

30. S.W.S. McKeever, *Thermoluminescence of Solids* (Cambridge University Press, New York, 1988)
31. A.J.J. Bos, Theory of thermoluminescence. Radiat. Meas. **41**, 45–56 (2007)
32. V. Pagonis, G. Kitis, C. Furetta, *Numerical and Practical Exercises in Thermoluminescence* (Springer, Berlin, 2006)
33. R. Chen, S.W.S. McKeever, *Theory of Thermoluminescence and Related Phenomenon* (World Scientific Press, Singapore, 1997)
34. M. Mashangva, M.N. Singh, T.B. Singh, Indian J. Pure Appl. Phys. **49**, 583–589 (2011)
35. F.M. Emena, N. Kulcu, A.N. Yazıcı, Eur. J. Chem. **1**(1), 28–32 (2010)
36. A.K. Parchur, R.S. Ningthoujam, Dalton Trans. **40**, 7590 (2011)
37. G.S. Rama Raju, J.Y. Park, H.C. Jung, B.K. Moon, J.H. Jeong, J.H. Kim, Curr. Appl. Phys. **9**, 92 (2009)
38. N.N. Yamashita, J. Phys. Soc. Jpn. **35**, 1089 (1973)
39. R. Pang, C. Li, L. Shi, Q. Su, J. Phys. Chem. Solids **70**, 303–306 (2009)
40. J. Kuang, Y. Liu, J. Zhang, J. Solid State Chem. **179**, 266–269 (2006)
41. Y. Chen, X. Cheng, M. Liu, Z. Qi, C. Shi, J. Lumin. **129**, 531–535 (2009)
42. A. Zukauskas, M.S. Shur, R. Gaska, *Introduction to Solid State Lighting* (Wiley, New York, 2002)
43. CIE 1931. International Commission on Illumination. Publication CIE no. 15 (E-1.3.1) 1931
44. C.S. McCamy, Color Res. Appl. **17**, 142–144 (1992)
45. I.P. Sahu, D.P. Bisen, N. Brahme, R.K. Tamrakar, R. Shrivastava, J. Mater. Sci.: Mater. Electron. (2015). doi:10.1007/s10854-015-3563-5
46. R. Rajeswari, C.K. Jayasankar, D. Ramachari, S. Surendra Babu, Ceram. Int. **39**, 7523–7529 (2013)
47. T. Erdem, S. Nizamogul, X.W. Sun, H.V. Demir, Opt. Express **18**, 340–347 (2010)
48. B.M. Mothudi, O.M. Ntwaeaborwa, S.S. Pitale, H.C. Swart, J. Alloys Compd. **508**, 262–265 (2010)
49. T. Aitasalo, J. Holsa, H. Jungner, M. Lastusaari, J. Niittykoski, J. Phys. Chem. B **110**, 4589–4598 (2006)
50. K.V.D. Eeckhout, P.F. Smet, D. Poelman, Materials **3**, 2536–2566 (2010)
51. D.R. Vij, *Luminescence of Solids* (Plenum Press, New York, 1998)
52. B.P. Chandra, J. Lumin. **131**, 1203–1210 (2011)
53. I.P. Sahu, D.P. Bisen, N. Brahme, R. Sharma, Res. Chem. Intermed. (2014). doi:10.1007/s11164-014-1767-6
54. I.P. Sahu, D.P. Bisen, N. Brahme, Lumin. J. Biol. Chem. Lumin. **30**(5), 526–532 (2015)
55. I.P. Sahu, D.P. Bisen, N. Brahme, L. Wanjari, R.K. Tamrakar, Res. Chem. Intermed. (2015). doi:10.1007/s11164-015-1929-1
56. B.P. Chandra, R.A. Rathore, Cryst. Res. Technol. **30**, 885–896 (1995)
57. I.P. Sahu, D.P. Bisen, N. Brahme, M. Ganjir, Lumin. J. Biol. Chem. Lumin. (2015). doi:10.1002/bio.2900
58. H. Zhang, H. Yamada, N. Terasaki, C.N. Xu, Thin Solid Films **518**, 610–613 (2009)
59. I.P. Sahu, D.P. Bisen, N. Brahme, R.K. Tamrakar, J. Lumin. **167**, 278–288 (2015)
60. H. Zhang, H. Yamada, N. Terasaki, C.N. Xu, Phys. E **42**, 2872–2875 (2010)